Green Synthesis and Electrochemical Study of Undoped and Doped Al₂O₃ Nanoparticles Using *Hibiscus rosa-sinensis* Leaves Extract

Farzana Haider*, Gul Asimullah Khan Nabi, Kiran Shah, Kafeel Ahmad Khan, and Haseeba Khan

Department of Chemistry, Bacha Khan University, Charsadda, 24420, Khyber Pakhtunkhwa, Pakistan

Abstract: *In the present work, nanoparticles of Al_2O_3, Cu-Al_2O_3, and Ni-Al_2O_3 were prepared using* Hibiscus rosa-sinensis *plant leaf extract through co-precipitation method. The prepared nanomaterials were characterized through TGA, EDX, SEM, UV-Vis, XRD, and FTIR instruments. The electrochemical behavior of Al_2O_3, Cu-Al_2O_3, and Ni-Al_2O_3 has been studied in DMF solution in the potential ranges from −1.5 to 1.5 V. The nanoparticles are thermally stable, according to the TGA, and the XRD patterns revealed that all the Al_2O_3, Cu-Al_2O_3, and Ni-Al_2O_3 particles were crystalline, with the mean sizes of 12.44, 34.61, and 31.63 nm, respectively. The cyclic voltammogram showed a cathodic peak (E_{pc}) at 0.49 V with an anodic counterpart (E_{pa}) at 0.49 V [$E_{1/2}$ = 1.748 V]. The optical band gaps of Al_2O_3, Cu-Al_2O_3, and Ni-Al_2O_3 were 3.8, 3.2 and 3.65 eV, owed a cathode. It is observed that the electrochemical behavior of Ni-Al_2O_3 was identical to that of Al_2O_3 and Cu-Al_2O_3. The anodic and cathodic peak values rise with the scan rate. The one-electron oxidation and reduction processes are reversible, as seen by the shifting cathodic peak value toward higher negative values. All cycles exhibit absorption has a constant anodic current. This result indicated the diffusion-based redox process.*

Keywords: *cyclic voltammogram; electrochemical behavior; co-precipitation method; Al_2O_3;* Hibiscus rosa-sinensis

■ INTRODUCTION

With potential applications in industries range starting cosmetics to electronics, the area of nanotechnology and nanoscience are rapidly expanding for biological, physical, chemical, and phenomena at the sub-atomic and atomic level [1-9]. Scientists are working hard to discover new technologies through nanosciences and nanotechnology that are involved in the creation of new materials with distinctive and better properties [10-12]. Nanoparticles (NPs) are synthetic particles produced by nanotechnology. NPs are increasingly being used in medicine, catalysis, cosmetics, dyes, and biosensing fields [6].

Outstanding physicochemical characteristics are found in NPs. When compared to other approaches, the synthesis and stability of NPs made from plants are both quicker and more stable [13]. Because there are so many plants, they are easily accessible, have an advantage over physical and chemical methods, and are simple to work with [14]. Additionally, there are no hazardous chemicals used in the production process. Natural capping agents derived from plants are useful for the production of NPs [15]. Doping is an important parameter used for NPs due to the reformation of physicochemical properties of metal oxide, which has large applications, especially in the electrochemical field [16].

Many processes are applied in the fabrication of NPs, together with electrochemistry, electrical devices, and catalysis [17]. In several branches of chemistry, cyclic voltammetry has emerged as a prominent and popular electro-analytical technique. By adjusting the electrode potential of an electrochemical cell, the redox reaction occurring on the electrode can be managed. Therefore, it is essential to study the electrochemical reactions that take place at electrode/electrolyte contact. By methodically analyzing the current-voltage data of a specific

electrochemical cell, cyclic voltammetry is a potent tool for studying the electrochemical behavior of a system. Voltammetric techniques are widely used by inorganic, physical, and biological chemists for a wide range of applications, including basic research on oxidation and reduction processes in various media, adsorption on surfaces, mechanisms of electron transfer and reaction, the kinetics of electron transfer processes, transport, speciation, and thermodynamic properties of solvated species [18].

The research interest of our group is to synthesize NPs using plants which are easily approachable, non-toxic, cheap, and safe. Scientists around the world are working on different plants for the synthesis of NPs, but the *Hibiscus rosa-sinensis* plant is not used up till now. The NPs were synthesized using the co-precipitation method using *H. rosa-sinensis* leaves extract in this study.

■ EXPERIMENTAL SECTION

Materials

Aluminium(III) nitrate, copper(II) nitrate, dimethyl sulfoxide (DMSO), nickel(II) nitrate, potassium chloride, and *H. rosa-sinensis* leaves were the ingredients employed in the manufacture of undoped and copper doped aluminium oxide (Al_2O_3) NPs. All chemicals came from the Sigma Aldrich firm and were utilized without any further processing. Aluminium(III) nitrate solution was prepared by taking 10 mL of aluminium(III) nitrate (1.06 M) and dissolved in 50 mL of deionized water to give 1 mM solution.

Instrumentation

A Gallenkamp thermal stirrer was used for the batch experiments (ZHWY-200B, ZHICHENG Analytical Co. Ltd). The metal solution was filtered through a Whatman filter paper No. 1 (Millipore Corp., Bedford, and Mass). A double-beam UV–visible spectrophotometer (UV-1800 240 V, Shimadzu Corporation) was used for the determination of NPs. Additionally, the particles underwent calcination in a muffle furnace (JFF 2000). The functional groups contained in the solution were examined by using FTIR (Perkin Elmer, resolution at 4 cm^{-1} in a range of diffusion reflect an assembly and KBr). Through EDX (INCA-200) and SEM (JSM-5910,

JEOL), respectively, the particles' elemental composition and surface morphology were examined. TGA was used to do the thermal studies of the particles (25–800 °C). Electrochemical characterizations of NPs were done by cyclic voltammetry. The cyclic voltammetric Potentiostate DY 2300 model was used to obtain a cyclic voltammogram. The electrochemical workstation consisted of a cell containing three electrodes: the calomel electrode was used as the reference electrode, the graphite electrode was used as the working electrode, and the gold electrode was used as the counter electrode. XRD analysis was performed at Cu Kα radiation = 1.5406, using the 2 ranges of 20–80° with a step width of 0.02" and step time of 2.40 s [19].

Procedure

Preparation of H. rosa-sinensis *leaves extract*

Fresh *H. rosa-sinensis* plant leaves were collected from District Charsadda. The leaves of the plant were washed several times with water to remove the dust particles and then sun-dried for 10 min to remove the residual moisture. After that, the leaves were shaded and dried for two weeks. Finally, dried leaves were ground into fine powder form. The extract was prepared by placing 20 g of finely powdered leaves, adding to 200 mL of double distilled water and boiling for 30 min. The extract was cooled to room temperature and filtered. The filtered extracts were stored in a refrigerator to be used for further experiments [20].

Synthesis of Al$_2$O$_3$ NPs

Using the green combustion approach and leaf extract from the *H. rosa-sinensis* plant as fuel, Al_2O_3 NPs were prepared. A 40 mL of aluminum(III) nitrate solution 1 mM was combined with 10 mL of *H. rosa-sinensis* plant extract. The muffle furnace was preheated at 200 ± 5 °C. The sample is then taken in a clay crucible and put in a muffle furnace. In roughly 2–3 min, the mixture burnt completely, yielding undoped Al_2O_3 NPs. The sample (ash) was then filtered to remove any leftover ash made from plant extract. The ash was cleaned with deionized water multiple times to remove impurities. The generated NPs were also calcinated for 2 h at 200 ± 5 °C to achieve purity. The characterization

results showing the Al_2O_3 NPs are fine and accurate, which were kept in an airtight container for further study [20].

Synthesis of copper-doped Al₂O₃ NPs

Using the green combustion technique and the leaf extract of *H. rosa-sinensis* as fuel, Cu-doped Al_2O_3 NPs were precipitated. In 40 mL of double-distilled water, 1 mM of aluminium(III) nitrate and 1.305 g of copper(II) nitrate trihydrate ($Cu(NO_3)_2 \cdot 3H_2O$) were combined with 10 mL of *H. rosa-sinensis* leaf extract. Using a magnetic stirrer and continual stirring at 2000 rpm, the solution was homogenized for 2 to 5 min. Firstly, the temperatures are set to $200 \pm 5\,°C$ and then start combustion. The sample was heated to $200 \pm 5\,°C$ in a muffle furnace before being placed in a clay crucible (with the aid of a long iron sample holder). Cu-doped Al_2O_3 NPs were produced as a result of the mixture burning within 2 to 3 min. Ashes from the plant extract were removed from the mixture through filtering, and pollutants were eliminated through rinsing with double-distilled water. To achieve purity, the produced NPs underwent 2 h calcination at $200 \pm 5\,°C$. The output, which was light greenish Cu-doped Al_2O_3 NPs kept in an airtight container, was satisfactory [19].

Synthesis of nickel-doped Al₂O₃ NPs

Utilizing the green combustion technique and *H. rosa-sinensis* leaf extract as fuel, Ni-doped Al_2O_3 NPs were created. A 10 mL of *H. rosa-sinensis* leaf extract was combined with 1 mM of aluminum(III) nitrate, 1.305 g of nickel(II) nitrate, and 40 mL of double distilled water. A magnetic stirrer was used to mix the solution continuously for 2 to 5 min at 2000 rpm. At the start of combustion, the temperature of the muffle furnace (Neycraf™ JFF 2000 furnace) is $200 \pm 5\,°C$. Following that, the sample was taken in a clay crucible and heated to $200 \pm 5\,°C$ in a muffle furnace. The mixture burnt entirely in 2 to 3 min, resulting in Ni-doped Al_2O_3 NPs. The resulting mixture was filtered to remove any ash from the plant extract before being cleaned with double-distilled water to remove any impurities. The synthesized NPs underwent a 2 h calcination procedure to obtain purity. As a result, fine, white Ni-doped Al_2O_3 NPs were created and stored in an airtight container [19].
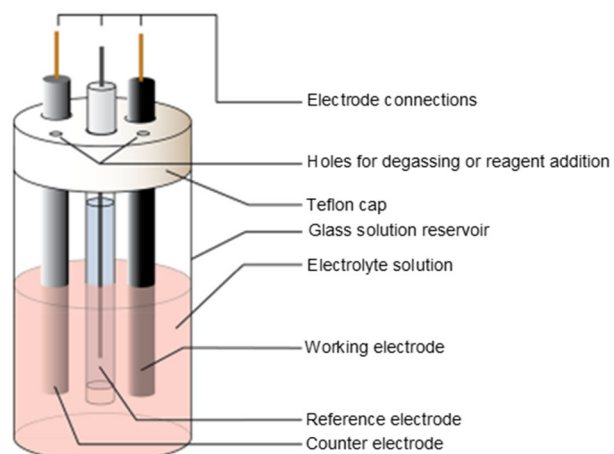
Fig 1. Schematic representation of an electrochemical cell for CV experiments

Procedure for electrochemical measurement (solution)

KCl solution was commonly employed as the inner solution for the reference electrode or as supporting electrolytes in the sample solution during cyclic voltammetry. Prepared Al_2O_3 NPs weighing 0.006 g were dissolved in 10 mL of DMSO solvent. A few drops of KCl solution were then added to this mixture. Similarly, for the 2 mM solution of Ni-doped Al_2O_3 NPs, the generated doped particle powder weighing 0.007 g was diluted in 10 mL of DMSO solvent. This solution was supplemented with a few drops of KCl solution. Likewise, for the 2 mM solution of Cu-doped Al_2O_3 NPs, the obtained doped particle powder weighing 0.007 g was diluted in 10 mL of DMSO solvent. A few drops of KCl solution were added to this combination. These carefully prepared solutions were integral to the subsequent electrochemical measurements.

Cyclic voltammetry

A schematic representation of an electrochemical cell is presented in Fig. 1.

■ **RESULTS AND DISCUSSION**

Characterization

SEM analysis

SEM analysis was employed in order to determine the size and morphologies of Al_2O_3, Cu-Al_2O_3 and Ni-Al_2O_3 NPs. SEM analysis of Al_2O_3, Cu-Al_2O_3, and Ni-

Al_2O_3 NPs. Fig. 2(a), (b) and (c) are taken within the range of 1 μm with the magnification of 10,000×, at an accelerating voltage of electron beam of 20 kV which are exhibited. Fig. 2(a), (b) and (c) shows the typical SEM images of Al_2O_3, $Cu-Al_2O_3$, and $Ni-Al_2O_3$ NPs. It is observed that Al_2O_3, $Cu-Al_2O_3$ and $Ni-Al_2O_3$ are of spherical morphology and have narrow diameter distributions (50–80 nm). However, Al_2O_3 NPs show aggregation (Fig. 2(a)), while $Cu-Al_2O_3$ and $Ni-Al_2O_3$ NPs are uneven and homogeneously scattered, as shown in Fig. 2(b, c).

EDX analysis

The EDX spectrum of Al_2O_3 demonstrates a strong link between O and Al with element weights of 59.35% and 40.65%, confirming the formation of Al_2O_3 NPs. Al_2O_3 NPs doped with Cu, the EDX spectrum reveals a prominent band of O, Al, S, Cl, and Cu with element weight of 58.79%, 38.67%, 0.82%, 0.35%, and 4.27% confirming the synthesis of Cu doped Al_2O_3 NPs. While Al_2O_3 NPs doped with Ni, the EDX spectrum reveals a prominent band of C, O, Al, K, and Ni with element weight of 8.04%, 46.22%, 39.67%, 0.72%, and 5.36% confirming the sample contains Ni doped Al_2O_3 NPs (see Table 1).
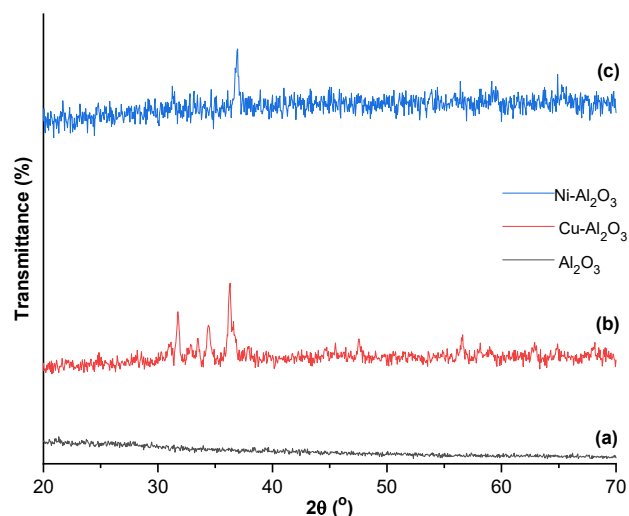
XRD analysis

Fig. 3(a), (b), and (c) shows the results of the XRD examination of Al_2O_3, $Cu-Al_2O_3$, and $Ni-Al_2O_3$ NPs. $Cu-Al_2O_3$, $Ni-Al_2O_3$, and Al_2O_3 sample crystallization took place at 350 °C calcinating temperatures. The samples exhibit high crystallinity, which shows that contaminants have been removed and a crystalline phase has formed. According to the XRD examination, tetragonal Al_2O_3 particles were produced with good crystallinity. The crystal sizes for $Cu-Al_2O_3$, $Ni-Al_2O_3$, and Al_2O_3 NPs, were

with diameters of 12.44, 34.61, and 31.63 nm, exhibit high crystallinity, which shows that contaminants have been

Table 1. EDX of Al_2O_3, $Cu-Al_2O_3$, and $Ni-Al_2O_3$

	Element	Weight (%)	Atomic (%)
Al_2O_3	O K	59.35	71.12
	Al K	40.65	28.88
	Totals	100.00	100.00
$Cu-Al_2O_3$	O K	55.89	68.51
	Al K	38.67	28.11
	S K	0.82	0.50
	Cl K	0.35	0.19
	Cu K	4.27	2.69
	Totals	100.00	100.00
$Ni-Al_2O_3$	C K	8.04	12.69
	O K	46.22	54.78
	Al K	39.67	27.88
	K K	0.72	0.35
	Ni K	5.36	4.29
	Totals	100.00	100.00

Fig 3. XRD Analysis of (a) Al_2O_3, (b) $Cu-Al_2O_3$, and (c) $Ni-Al_2O_3$
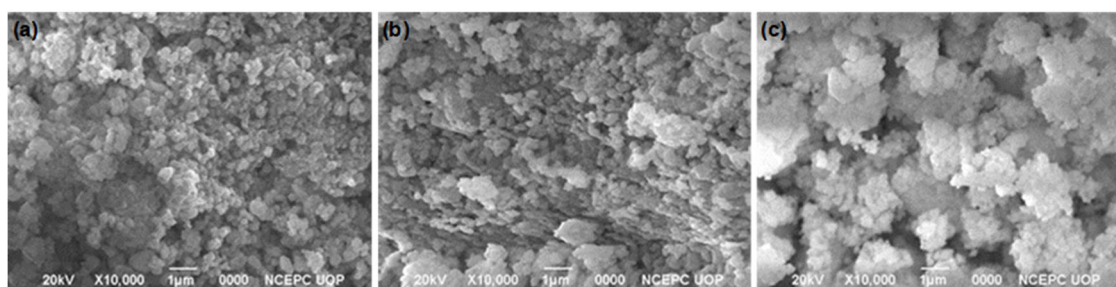
Fig 2. SEM images of (a) Al_2O_3, (b) $Cu-Al_2O_3$, and (c) $Ni-Al_2O_3$

removed and a crystalline phase has formed. According to the XRD examination, tetragonal Al_2O_3 particles were produced with good crystallinity. The crystal sizes for Cu-Al_2O_3, Ni-Al_2O_3, and Al_2O_3 NPs, were with diameters of 12.44, 34.61, and 31.63 nm, respectively. It was discovered that the amount of additive had a significant impact on the nanocrystalline Al_2O_3 crystalline size effect. The growth in crystallite size is caused by the doping's continued addition. The increase in crystallite size with the increased addition of the doped. The observed pattern has a number of sharp peaks orientation in the planes (110), (020), (101), (022), (200), (111), (211), (220), (002), (310), (112), (301), and (202) at different angles (2θ) indicating that higher crystallinity of the material. No peaks of extra impurity crystalline phases have been detected. All strong and sharp diffraction peaks obtained are approved by the formation of Al_2O_3. The experimental XRD pattern shows diffraction lines of cassiterite Al_2O_3 (ICDD PDF no. 88-0287). The crystallite size (D) was calculated by the measurement of the diffraction line and applying the Debye Scherrer formula, Eq. (1) [21];

$$D = \frac{0.94\lambda}{\beta\cos\theta} \qquad (1)$$

where λ is the wavelength of α radiations, β the full width at half maximum of the peaks corresponding to the plane, and θ the angle obtained from 2θ value corresponding to a maximum intensity peak in the XRD pattern. The size of crystalline NPs can be estimated by the amount by which the X-ray line is sharp.

FTIR analysis

Fig. 4 shows the Fourier transform infrared (FTIR) spectra of the synthesized Al_2O_3 as well as doped Cu-Al_2O_3 and Ni-Al_2O_3 NPs. The FTIR spectrum of Al_2O_3 and Cu-Al_2O_3 and Ni-Al_2O_3 NPs shows the carbonyl group (C=O), stretching C=C aromatic ring, C-OH stretching vibrations, and C-I hydrogen compound at 1653, 1416.34, 1329.98, 1043.71, 814.21, and 541.53 cm^{-1}, respectively [22]. The FTIR analysis clearly shows that plant chemicals are adsorbed on the surface of metal NPs and act as capping, stabilizing, and protecting agents, as shown in Fig. 4(a-c).

TGA analysis

Fig. 5(a), (b) and (c) shows the TGA analysis for Al_2O_3,

Cu-Al_2O_3, and Ni-Al_2O_3 NPs was performed within the temperature range (25–800 °C). This study was performed in the nitrogen environment at a speed of 15 °C/min to analyze the weight loss of the samples. The weight loss caused by moisture was excluded at 100 °C. Thus, the total weight loss in Cu-Al_2O_3 was 44.57% up to 800 °C, 21.22% in Ni-Al_2O_3, and 62.66% in Al_2O_3 NPs were observed. Cu-Al_2O_3 and Ni-Al_2O_3 loosed less weight due to the presence of more functional groups [23-24].
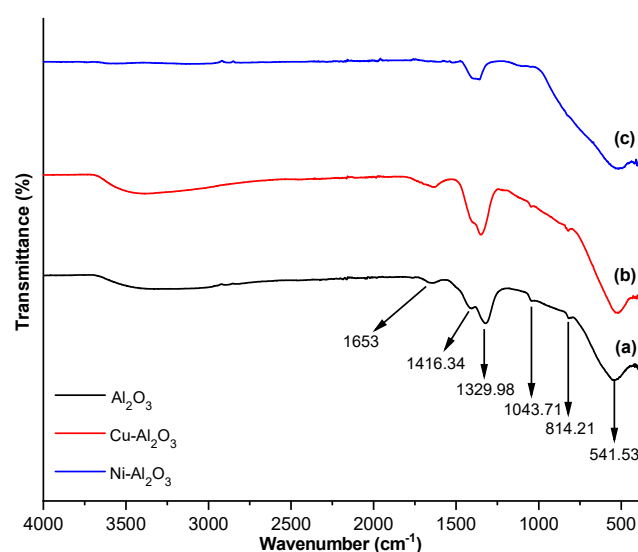

Fig 4. FTIR spectra of (a) Al_2O_3 and (b) Cu-Al_2O_3, (c) Ni-Al_2O_3 NPs
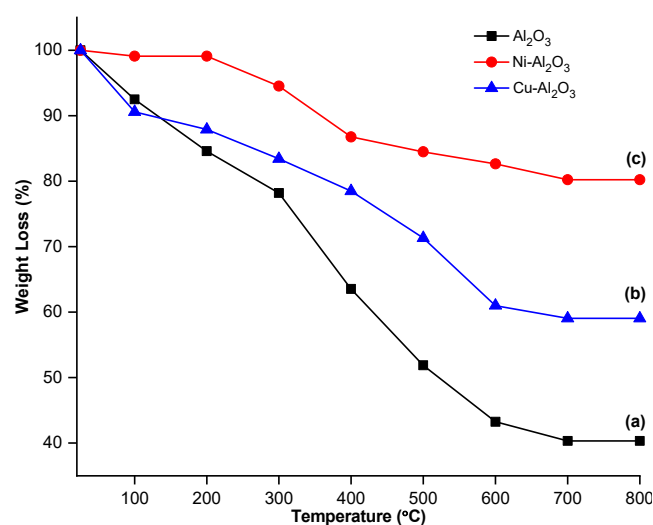
Fig 5. Thermal gravimetric analysis of (a) Al_2O_3 and (b) Cu-Al_2O_3, (c) Ni-Al_2O_3 NPs

UV-Vis and Optical Band Energy

UV-Vis absorption spectra and optical band gap energy of Al_2O_3, $Cu-Al_2O_3$, and $Ni-Al_2O_3$. The spectra show strong absorption peaks at 303, 324 and 300 nm for Al_2O_3, $Cu-Al_2O_3$ and $Ni-Al_2O_3$. This is due to electron photoexcitation from the valence band to the conduction band. The direct optical band gap energy (E_g) of Al_2O_3, $Cu-Al_2O_3$ and $Ni-Al_2O_3$ is calculated using the Tauc relation, Eq. (2) and (3);

$$(\alpha h\nu)^2 = \beta(h\nu - E_g) \qquad (2)$$

where β is constant, and α is the absorption coefficient, and it is determined using the following relation:

$$\alpha(\lambda) = 2.303TA \qquad (3)$$

where A and T are the absorbances and the thickness of the prepared sample, respectively. Fig. 6 represents the plot of $(\alpha h\nu)^2$ against $h\nu$ of Al_2O_3, $Cu-Al_2O_3$ and $Ni-Al_2O_3$. The direct optical band gap energy E_g is calculated by extrapolating the linear portion of the plot with photon energy ($h\nu$) [25]. As shown values of E_g are 3.8, 3.2 and 3.65 eV.
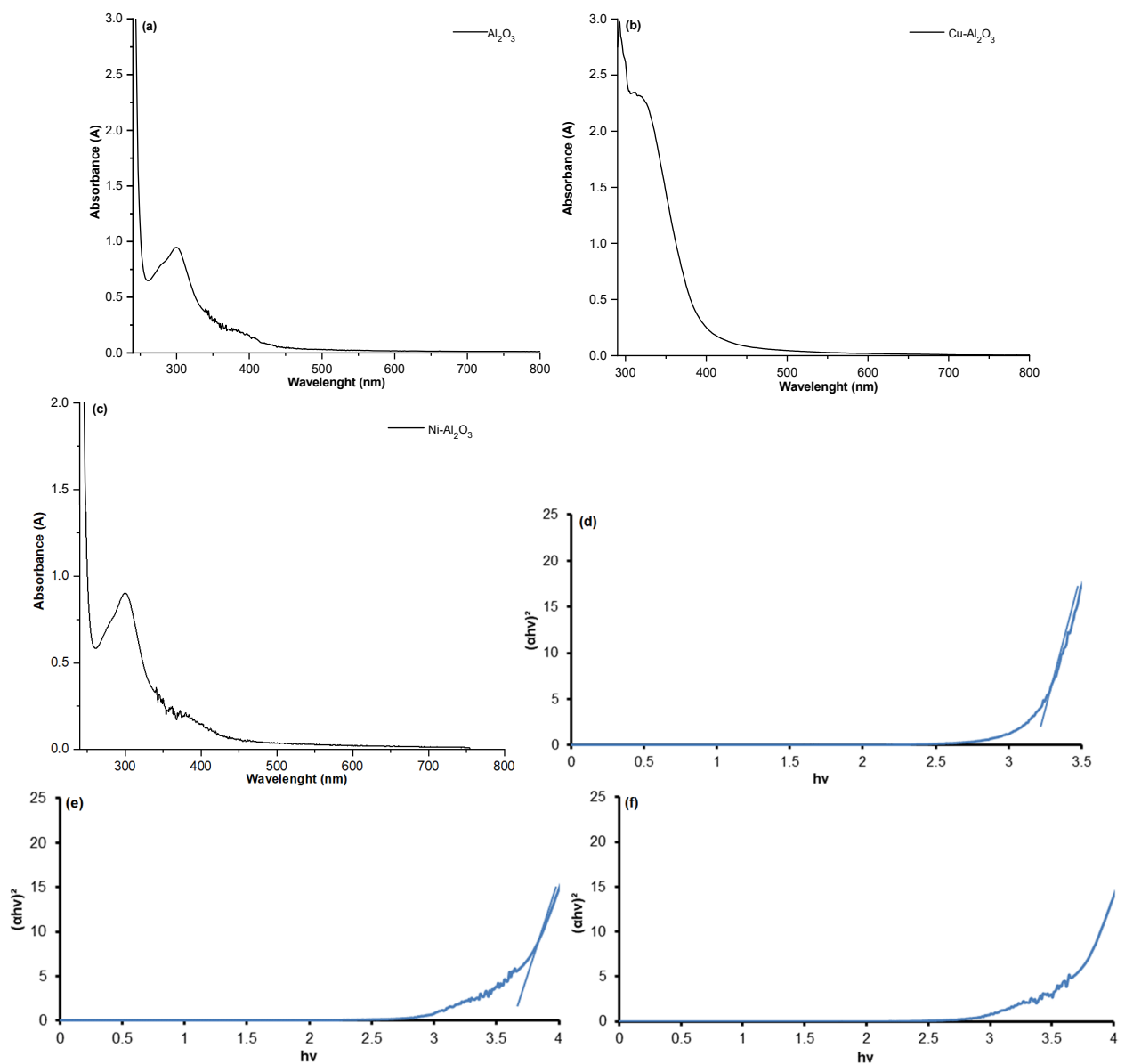
Fig 6. UV-Vis Spectra of (a) Al_2O_3, (b) $Cu-Al_2O_3$ and (c) $Ni-Al_2O_3$ and optical band gap of (d) Al_2O_3, (e) $Cu-Al_2O_3$ and (f) $Ni-Al_2O_3$

Electrochemical Studies

The electrochemical behavior of the metal NPs undoped Al_2O_3, doped $Cu-Al_2O_3$ and $Ni-Al_2O_3$ have been studied in DMF solution. Fig. 7 shows the cyclic voltammogram of metal NPs Al_2O_3, doped $Cu-Al_2O_3$ and $Ni-Al_2O_3$, in DMF solution with potential ranges of −1.5 to 1.5 V. The electrochemically irreversible reduction peak observed at 0.524 V is due to the reduction of Al_2O_3, doped $Cu-Al_2O_3$ and $Ni-Al_2O_3$ center. This value is in agreement with those observed in the related Al_2O_3, doped $Cu-Al_2O_3$ and $Ni-Al_2O_3$ Schiff base complexes. The irreversibility of the redox processes can be attributed to the instability of the reduced species in DMF solvent. By expanding the cyclic voltammogram potential range and monitoring the cyclic voltammogram of 1, 2 and 3 from −1.5 to 1.5 V, one reduction wave at −1.5 to 1.5 V. The cyclic voltammogram shows a cathodic peak (E_{pc}) at 0.49 V with an anodic counterpart (E_{pa}) at 0.49 V [$E_{1/2} =$ 1.748 V]. The electrochemical behavior and the data are in agreement with those reported for related Al_2O_3, doped $Cu-Al_2O_3$ and $Ni-Al_2O_3$ [26]. From the cyclic voltammogram, it is clear that the electroactive species reduced and then oxidized. In the forward scan, the species lost electrons and becomes reduced. In reverse scan, the species gained electrons and became oxidized. The oxidation and reduction take place on the working electrode. At a 2 V/s scan rate, the voltammogram was completed very quickly, which showed the electrical energy stored in electroactive species.
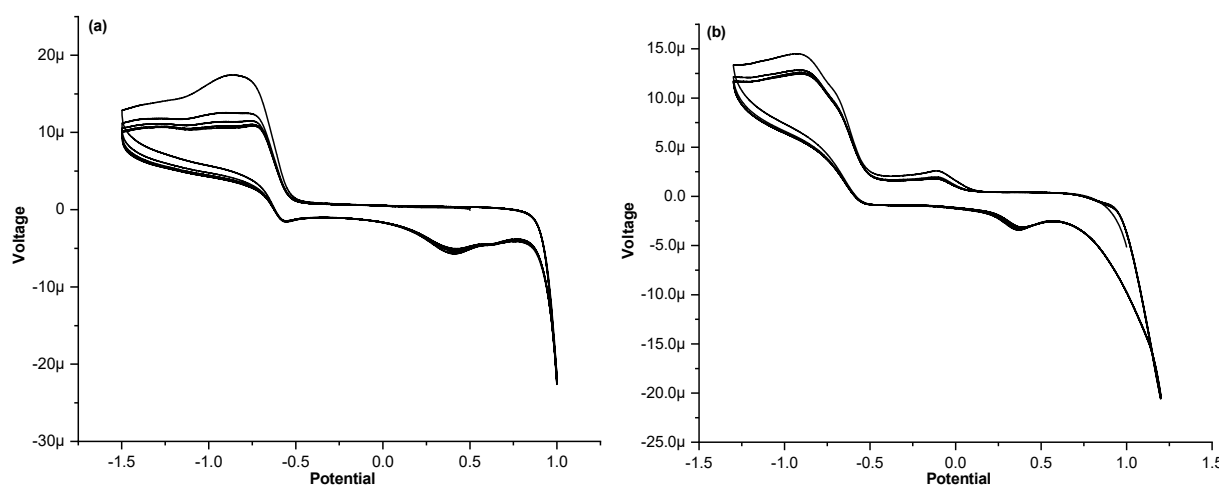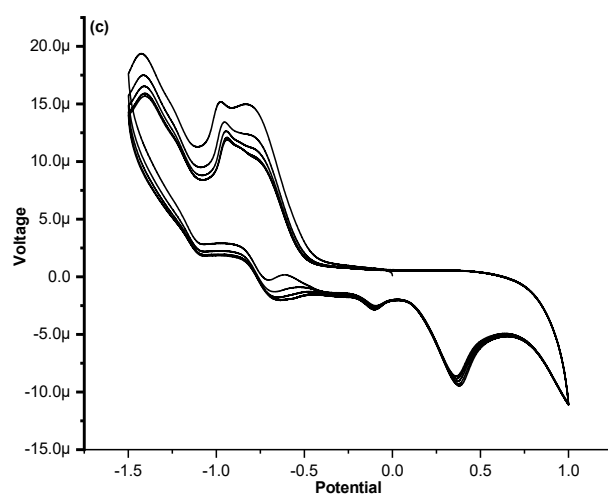
Voltammogram of Polycyclic

To obtain 5 cycles voltammogram for Al_2O_3, $Cu-Al_2O_3$ and $Cu-Al_2O_3$ at room temperature and pressure, the potentiostat was operated at 0.05 V with a potential range of −1.5 V to +1.5 V. The redox process was based on adsorption-regulated or diffusion controlled, which multicycles assist in explaining. If the anodic current drops in several cycles, adsorption takes place. The redox process was diffusion-based if the anodic current continued to flow unaltered [27].

Fig. 8(a) displays the Al_2O_3 voltammogram with 5 back-to-back cycles and a scan rate of 0.05 V. The voltammogram demonstrated that the anodic current was not constant, proving that absorption was taking place. All cycles that exhibit absorption have a constant anodic
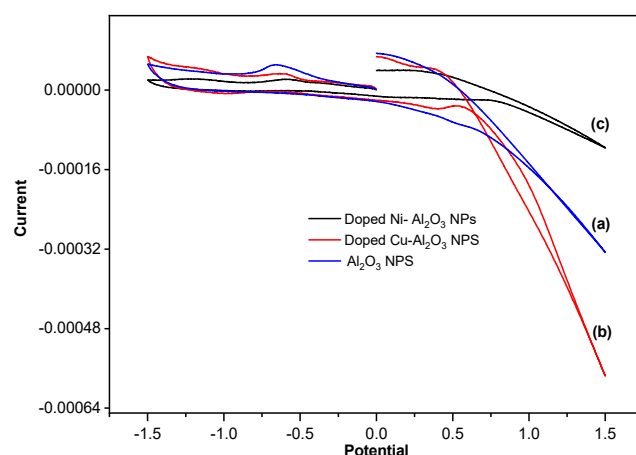
Fig 7. Cyclic voltammogram of (a) Al_2O_3, (b) $Cu-Al_2O_3$, and (c) $Ni-Al_2O_3$ NPs with scan rate of 2 V/s

920

Indones. J. Chem., 2023, 23 (4), 913 - 923

Fig 8. Cyclic voltammogram of (a) Al_2O_3, (b) $Cu-Al_2O_3$ and (c) $Ni-Al_2O_3$ at 0.05 V scan rate

current. The values of anodic and cathodic currents are essentially constant. This showed that the redox process was diffusion based.

At a scan rate of 50 mV, Fig. 8(b) shows a 5 cyclic voltammogram of $Cu-Al_2O_3$. The voltammogram made it evident that the anodic current stayed constant, indicating a diffusion control redox mechanism. Because each $Cu-Al_2O_3$ molecule had a similar amount of anode surface area to employ, the current stayed constant. The intricate molecule does not stick to the anode's surface but is desorbed from the surface.

The potentiostat was operated for 5 cyclic voltammograms at a 0.05 V scan rate for $Ni-Al_2O_3$ in order to demonstrate the adsorption base redox process. The anodic current remained constant, as seen in Fig. 8(c), demonstrating a diffusion-controlled redox

mechanism. Each $Ni-Al_2O_3$ molecule had a similar amount of anode surface area to employ, making the current stay constant. The intricate molecule does not adhere to the anode's surface, because each complicated molecule readily donates electrons at the anode, and the current was produced.

Voltammogram of Different Scan Rates

The Al_2O_3 voltammogram was displayed in Fig. 9(a) at various scan speeds. The cathodic potential value changes to the negative side as the scan rate value rises, whereas the anodic peak goes to the positive side. Reversible mechanisms of oxidation and reduction existed because the heterogeneous rate constant values are high.

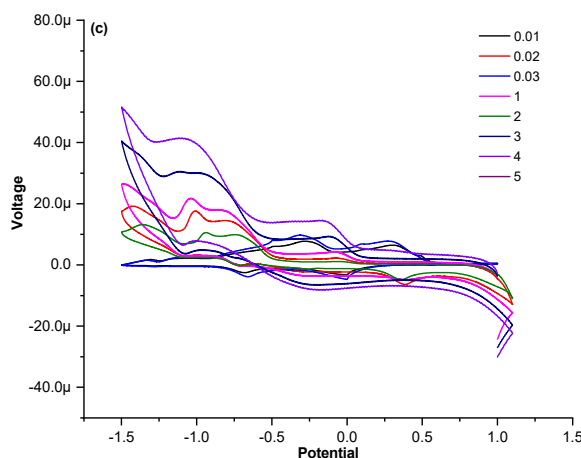The voltammogram of $Cu-Al_2O_3$ at various scan speeds is shown in Fig. 9(b). With an increase in scan rate,

Indones. J. Chem., 2023, 23 (4), 913 - 923

921
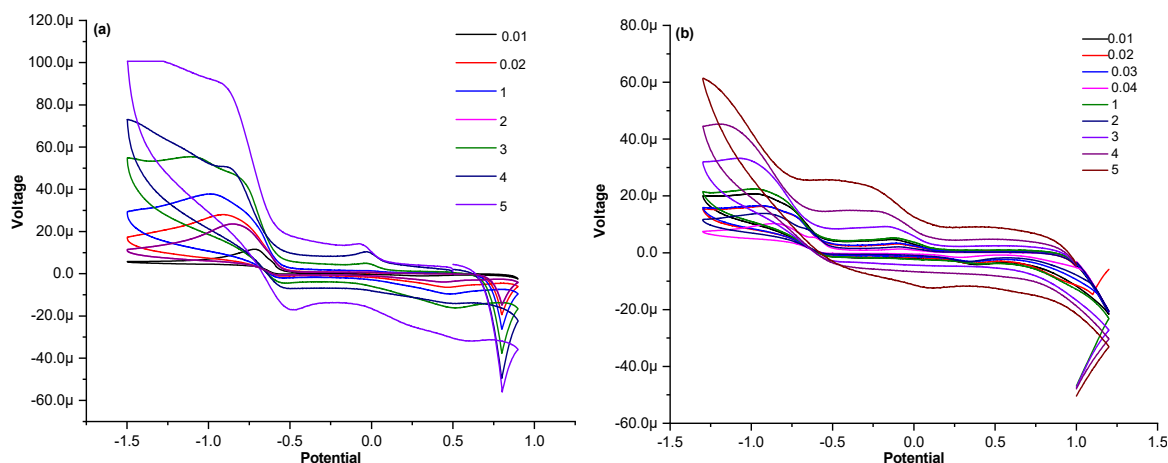
Fig 9. Voltammogram of (a) Al_2O_3, (b) $Cu\text{-}Al_2O_3$ and (c) $Ni\text{-}Al_2O_3$ at 0.05V scan rate at various scan rates

the anodic potential value shifts toward a more positive value and the cathodic potential value toward a more negative side. It demonstrated that the mechanism is reversible. The $Ni\text{-}Al_2O_3$ voltammogram was displayed in Fig. 9(c) at various scan speeds. The electrochemical behavior of $Ni\text{-}Al_2O_3$ was identical to that of Al_2O_3 and $Cu\text{-}Al_2O_3$. The anodic and cathodic peak values rise with the scan rate. The one-electron oxidation and reduction processes are reversible, as seen by the shifting cathodic peak value toward higher negative values.

■ CONCLUSION

The present work presented using *H. rosa-sinensis* plant leaf extract, Al_2O_3, $Cu\text{-}Al_2O_3$, and $Ni\text{-}Al_2O_3$ NPs were prepared through co-precipitation method. The synthesized particles were analyzed using different techniques EDX, XRD, FTIR, and UV-Vis. The phase structure and surface area of the prepared photocatalyst were investigated using XRD. The shape and composition of Al_2O_3, $Cu\text{-}Al_2O_3$, and $Ni\text{-}Al_2O_3$ NPs were analyzed through SEM and EDX techniques. The cyclic voltammogram shows a cathodic peak (E_{pc}) at 0.49 V with an anodic counterpart (E_{pa} at 0.49 V [$E_{1/2}$ = 1.748 V] within potential ranges from −1.5 to 1.5 V. The electrochemical behavior and the data are in agreement with those reported for related Al_2O_3, $Cu\text{-}Al_2O_3$, and $Ni\text{-}Al_2O_3$. It is noted that the intricate molecule does not adhere to the anode's surface as each molecule readily donates electrons at the anode, and the current was produced.

■ REFERENCES

[1] Vinardell, M.P., Sordé, A., Díaz, J., Baccarin, T., and Mitjans, M., 2015, Comparative effects of macro-sized aluminum oxide and aluminum oxide nanoparticles on erythrocyte hemolysis: Influence of cell source, temperature, and size, *J. Nanopart. Res.*, 17 (2), 80.

[2] Huguet-Casquero, A., Gainza, E., and Pedraz, J.L., 2021, Towards Green Nanoscience: From extraction to nanoformulation, *Biotechnol. Adv.*, 46, 107657.

[3] Pathak, M., Pathak, P., Khalilullah, H., Grishina, M., Potemkin, V., Kumar, V., Majee, R., Ramteke, P.W., Abdellattif, M.H., Shahbaaz, M., and Verma, A., 2021, Green synthesis of silver nanoformulation of *Scindapsus officinalis* as potent anticancer and predicted anticovid alternative: Exploration via experimental and computational methods, *Biocatal. Agric. Biotechnol.*, 35, 102072.

[4] Ingle, A.P., Duran, N., and Rai, M., 2014, Bioactivity, mechanism of action, and cytotoxicity of copper-based nanoparticles: A review, *Appl. Microbiol. Biotechnol.*, 98 (3), 1001–1009.

[5] Erenler, R., Gecer, E.N., Hosaflioglu, I., and Behcet, L., 2023, Green synthesis of silver nanoparticles using *Stachys spectabilis*: Identification, catalytic degradation, and antioxidant activity, *Biochem. Biophys. Res. Commun.*, 659, 91–95.

[6] Schrand, A.M., Rahman, M.F., Hussain, S.M., Schlager, J.J., Smith, D.A., and Syed, A.F., 2010, Metal-based nanoparticles and their toxicity assessment, *WIREs Nanomed. Nanobiotechnol.*, 2 (5), 544–568.

[7] Brouwer, H., Van Oijen, F.L.N., and Bouwmeester, H., 2023, "Potential human health effects following exposure to nano- and microplastics, lessons learned from nanomaterials" in *Present Knowledge in Food Safety*, Eds. Bouwmeester, H., Knowles, M.E., Anelich, L.E., Boobis, A.R., and Popping, B., Academic Press, Cambridge, US, 590–605.

[8] O'Shaughnessy, P.T., 2013, Occupational health risk to nanoparticulate exposure, *Environ. Sci.: Processes Impacts*, 15 (1), 49–62.

[9] Luyts, K., Napierska, D., Nemery, B., and Hoet, P.H.M., 2013, How physico-chemical characteristics of nanoparticles cause their toxicity: complex and unresolved interrelations, *Environ. Sci.: Processes Impacts*, 15 (1), 23–38.

[10] Malakar, R., Kanel, S.R., Ray, C., Snow, D.D., and Nadagouda, N.M., 2021, Nanomaterials in the environment, human exposure pathway, and health effects: A review, *Sci. Total Environ.*, 759, 143470.

[11] Ma, N.L., Zhang N., Yong, W.T.L., Misbah, S., Hashim, F., Soon, C.F., Lim, G.P., Peng, W., and Sonne, C., 2023, Use, exposure and omics characterisation of potential hazard in nanomaterials, *Mater. Today Adv.*, 17, 100341.

[12] Monisha, B., Sridharan, R., Kumar, P.S., Rangasamy, G., Krishnaswamy, V.G., and Subhashree, S., 2023, Sensing of azo toxic dyes using nanomaterials and its health effects - A review, *Chemosphere*, 313, 137614.

[13] Karlsson, H.L., Cronholm, P., Hedberg, Y., Tornberg, M., De Battice, L., Svedhem, S., and Wallinder, I.O., 2013, Cell membrane damage and protein interaction induced by copper containing nanoparticles–Importance of the metal release process, *Toxicology*, 313 (1), 59–69.

[14] Aruna, A., Nandhini, R., Karthikeyan, V., and Bose, P., 2014, Synthesis and characterization of silver nanoparticles of insulin plant (*Costus pictus* D. Don) leaves, *Asian J. Biomed. Pharm. Sci.*, 4 (34), 1–6.

[15] Khan, M.Z.H., Tareq, F.K., Hossen, M.A., and Roki, M.N.A.M., 2018, Green synthesis and characterization of silver nanoparticles using *Coriandrum sativum* leaf extract, *Int. J. Eng. Sci.*, 13 (1), 158–166.

[16] Pirasteh, M., Isfahani, T.M., and Pourghobadi, Z., 2022, Electrochemical codeine sensor based on carbon paste electrode/HKUST-1, *Mater. Res. Express*, 9, 095008.

[17] Ken, D.S., and Sinha, A., 2020, Recent developments in surface modification of nano zero-valent iron (nZVI): Remediation, toxicity and environmental impacts, *Environ. Nanotechnol., Monit. Manage.*, 14, 100344.

[18] Joshi, P.S., and Sutrave, D.S., 2018, A brief study of cyclic voltammetry and electrochemical analysis, *Int. J. ChemTech Res.*, 11 (9), 77–88.

[19] Naz, F., Nabi, G.A.K., Nawaz, A., Ali, S., and Siddique, M., 2022, A novel approach for the photocatalytic degradation of binary dyes mixture using SnO_2 nanoparticles as a catalyst, *J. Cluster Sci.*, 34 (4), 2047–2066.

[20] Sumesh, K.R., and Kanthavel, K., 2019, Green synthesis of aluminium oxide nanoparticles and its applications in mechanical and thermal stability of hybrid natural composites, *J. Polym. Environ.*, 27 (10), 2189–2200.

[21] Tas Anli, S., Ebeoglugil, M.F., and Celik, E., 2020, Effect of dopant elements on structure and morphology of SnO_2 nanoparticles, *J. Aust. Ceram. Soc.*, 56 (2), 403–411.

[22] Nasrollahzadeh, M., Issaabadi, Z., and Sajadi, S.M., 2019, Green synthesis of Cu/Al_2O_3 nanoparticles as efficient and recyclable catalyst for reduction of 2,4-dinitrophenylhydrazine, Methylene blue and Congo

Indones. J. Chem., 2023, 23 (4), 913 - 923

923

red, *Composites, Part B*, 166, 112–119.

[23] Changmai, M., Priyesh, J.P., and Purkait, M.K., 2017, Al_2O_3 nanoparticles synthesized using various oxidizing agents: Defluoridation performance, *J. Sci.: Adv. Mater. Devices*, 2 (4), 483–492.

[24] Younes, N., Kashyout, A.E.H.B., Shoueir, K., and El-Kemary, M., 2022, Palladium doped tungsten oxide nanoparticle nanocomposite for sensitive detection of CO_2 and LPG gases, *J. Mater. Res. Technol.*, 19, 2633–2644.

[25] Ismail, R.A., Zaidan, S.A., and Kadhim, R.M., 2017, Preparation and characterization of aluminum oxide nanoparticles by laser ablation in liquid as passivating and anti-reflection coating for silicon photodiodes, *Appl. Nanosci.*, 7 (7), 477–487.

[26] Chebout, O., Trifa, C., Bouacida, S., Boudraa, M., Imane, H., Merzougui, M., Mazouz, W., Ouari, K., Boudaren, C., and Merazig, H., 2022, Two new copper(II) complexes with sulfanilamide as ligand: Synthesis, structural, thermal analysis, electrochemical studies and antibacterial activity, *J. Mol. Struc.*, 1248, 131446.

[27] Raccichini, R., Amores, M., and Hinds, G., 2019, Critical review of the use of reference electrodes in Li-ion batteries: A diagnostic perspective, *Batteries*, 5 (1), 12.